Electrochemistry

The Electrochemical Society of Japan

Received: April 13, 2017
Accepted: June 21, 2017
Published: October 5, 2017

http://dx.doi.org/10.5796/electrochemistry.85.675

Article

Electrochemistry, **85(10)**, 675–679 (2017)

Electrochemical Sodiation-desodiation of Maricite $NaFePO_4$ in Ionic Liquid Electrolyte

Jinkwang HWANG,[a] Kazuhiko MATSUMOTO,[a,*] Toshiyuki NOHIRA,[b] and Rika HAGIWARA[a]

[a] *Graduate School of Energy Science, Kyoto University, Yoshida-honmachi, Sakyo-ku, Kyoto 606-8501, Japan*
[b] *Institute of Advanced Energy, Kyoto University, Gokasho, Uji 611-0011, Japan*

* *Corresponding author: k-matsumoto@energy.kyoto-u.ac.jp*

ABSTRACT

Maricite $NaFePO_4$ (m-$NaFePO_4$) has long been regarded as an electrochemically inactive material because Na^+ cannot overcome the activation energy of its diffusion pathways for sodium extraction and insertion in the structure. In this study, the charge-discharge behavior of m-$NaFePO_4$ ball-milled to the nano-size level was investigated in Na[FSA]-[C_3C_1pyrr][FSA] (C_3C_1pyrr = *N*-methyl-*N*-propylpyrrolidinium and FSA = bis(fluorosulfonyl)amide) ionic liquid electrolyte at 298 and 363 K. The charge-discharge performance was improved upon elevating the operational temperature, possibly because of the enhanced Na^+ diffusion in the maricite structure and in the electrolyte, and improved electrode reaction. The reversible capacity at 363 K increased with consecutive cycles and reached 100 mAh g^{-1} with nearly 100% coulombic efficiency in the 120th cycle at the C/2 rate. Ex-situ XRD results confirmed the preservation of the maricite phase after cycling, which may indicate that the practical capacity for maricite $NaFePO_4$ without amorphization. By reconsideration of electrochemically inactive materials for intermediate temperature operation, this study suggests the possibility of extending the range of available positive electrode materials for sodium secondary batteries.

Keywords : Sodium Secondary Battery, Ionic Liquid, Energy Storage, Maricite

1. Introduction

A number of portable devices adopting Li secondary batteries have been commercialized owing to their high performance, enabling their high share in the global rechargeable battery market.[1–3] The global demands for secondary batteries are growing exponentially, and the price of Li resources is accordingly rising every year.[4,5] Consequently, Na secondary batteries have received considerable attention as suitable alternatives to solve the critical problem concerning the lack of natural abundance for Li resources and the escalating price of Li. It is possible to design relatively high performance secondary batteries using a Na^+ shuttle owing to its low redox potential ($E^o_{Na+/Na} = -2.71$ V vs. SHE; $E^o_{Li+/Li} = -3.04$ V vs. SHE) and second smallest ionic radius in the group 1 elements (1.02 Å for Na^+ and 0.76 Å for Li^+ in the case of 6-coordination[6]). On the other hand, currently known Na secondary batteries do not exceed the performance of Li secondary batteries, and therefore, cost effectiveness is an important driver for the development of Na secondary batteries. For this purpose, electrode materials need to be prepared without using trace elements such as Cr, Co and Ni.[7]

Positive electrode materials based on Fe^{3+}/Fe^{2+} redox have enormous merits for Na secondary batteries because of their natural abundance and low cost. In particular, $NaFePO_4$ is composed of abundant elements and has the highest theoretical capacity of 155 mAh g^{-1} in the iron-based phosphate family (e.g. Na_2FePO_4F = 120 mAh g^{-1}, $Na_2FeP_2O_7$ = 97 mAh g^{-1}, and $Na_4Fe(PO_4)_2P_2O_7$ = 130 mAh g^{-1}).[8–13] Olivine $NaFePO_4$ is known to have two polymorphs (triphylite and maricite).[14] Triphylite $NaFePO_4$ is commonly called olivine, which is isostructural to olivine $LiFePO_4$. This material was prepared by a chemical and electrochemical Li-Na exchange process (delithiation of $LiFePO_4$ and sodiation of $FePO_4$).[15,16] Triphylite $NaFePO_4$ delivers a practical reversible capacity of 120 mAh g^{-1} based on Fe^{3+}/Fe^{2+} redox activity.[15] Maricite $NaFePO_4$ (m-$NaFePO_4$) is a thermodynamically stable phase and is synthesized by a conventional solid-state method.[14] This polymorph was previously believed to be electrochemically inactive as a positive electrode material for Na secondary batteries because the network of FeO_6-FeO_6 (edge-sharing) and PO_4-FeO_6 (corner-sharing) units hinder effective diffusion of Na^+.[8,14–17] A recent report, however, revealed that nano-sized m-$NaFePO_4$ can be used as a positive electrode material.[16] This finding was related to the transformation of the m-$NaFePO_4$ phase into an amorphous structure during the first charge. Although two preferable pathways for Na^+ diffusion were proposed, the activation barriers in the maricite structure along the diffusion paths are too high to overcome at room temperature; therefore, amorphization is required for Na^+ diffusion.[16]

Despite recently highlighted safety issues, most of the research on Na secondary batteries is still conducted using organic electrolytes.[18,19] Organic electrolytes, however, can only be used in a limited temperature range (<60°C) owing to their flammability and volatility.[20–22] On the other hand, ionic liquids (ILs) consist of only cations and anions and have several benefits, including low flammability, negligible vapor pressure, high thermal stability, and wide electrochemical window as electrolytes.[23–26] Thermally and chemically stable IL electrolytes facilitate operation of sodium secondary batteries at elevated temperatures. Operation of batteries at elevated temperatures can be realized in environments at intermediate temperatures, which exist not only near industrial surroundings but also residential areas, where the latent heat from machines, automobile engines, and domestic boilers can be exploited. Moreover, the elevated operating temperatures of IL electrolytes have been reported to be very effective for improving the charge-discharge performance of $NaCrO_2$ positive electrodes, and hard carbon and Sn alloy negative electrodes.[27–33] In the case of a Na/$Na_2FeP_2O_7$ cell using IL electrolytes, high rate performance and outstanding cyclability have been achieved at 363 K.[34,35]

In this paper, we report the charge-discharge behavior of m-$NaFePO_4$ positive electrode in Na[FSA]-[C_3C_1pyrr][FSA] (FSA^- = bis(fluorosulfonyl)amide anion and $C_3C_1pyrr^+$ = *N*-propyl-*N*-methylpyrrolidinium cation) electrolyte at intermediate-temperatures (e.g. ionic conductivity is 17.3 mS cm^{-1} at 363 K for Na[FSA]-[C_3C_1pyrr][FSA] = 30:70 mol%[26]). Elevating the operating temperature up to 363 K is expected to improve Na^+ diffusion in the solid-state and in the electrolyte, and enhance the electrode reaction, thus converting an electrochemically inactive m-$NaFePO_4$ to an active material.

2. Experimental

The powdery sample of m-$NaFePO_4$ was synthesized by a conventional solid-state method.[14] Stoichiometric amounts of Na_2CO_3 (Wako Pure Chemical Industries, purity 99.8%), $FeC_2O_4{\cdot}2H_2O$ (Wako Pure Chemical Industries, purity 99%) and $(NH_4)_2HPO_4$ (Wako Pure Chemical Industries, purity > 99%) were used without further purification and thoroughly mixed by wet planetary ball milling in acetone for 12 hr (600 rpm). The ball-milled mixture was collected by flushing with acetone, followed by drying for 24 hr at 393 K. The mixture was well ground using a mortar and pestle after the drying procedure. The precursor mixture was then calcined at 623 K for 3 hr and then baked at 873 K for 12 hr under Ar atmosphere.

The pure phase of m-$NaFePO_4$ was confirmed by X-ray diffraction (XRD) using a Rigaku Smart Lab diffractometer with Cu-*Kα* radiation (40 kV and 30 mA) and Rietveld refinement was performed using the FullProf software.[36] The morphology of the as prepared m-$NaFePO_4$ and the ball-milled sample was observed by field-emission scanning electron microscopy (FE-SEM, Hitachi SU-8020). Ex-situ XRD measurements were performed using an airtight XRD sample holder by the Rigaku Smart Lab. After electrochemical measurements, cells were disassembled in an Ar-filled glovebox and the m-$NaFePO_4$ electrodes were washed three times with super dehydrated tetrahydrofuran (Wako Pure Chemical Industries, water content ≤ 10 ppm) in the glovebox. Each dried electrode was loaded onto the airtight XRD sample holder for the measurement.

The electrochemical studies of m-$NaFePO_4$ were performed with 2032-type coin cells at 298 and 363 K. The prepared m-$NaFePO_4$ and Super C65 carbon were mixed by planetary ball milling (Fritsch Pulverisette 7 Premium Line) at a ratio of 80:20 wt% for 6 hr under Ar atmosphere. The materials were loaded into a ball-milling container and capped in an Ar-filled glove box to avoid contact with moisture and oxygen. The ball-milled mixture, Super C65, and PTFE (80:10:10 wt%) were mixed using a mortar and pestle in the glovebox. Approximately 4 mg cm^{-2} of the mixed material was pressed on Al mesh and used as a positive electrode. Metallic sodium (Aldrich, purity 99.95%) was cut into a disk with a diameter of 16 mm and used as a electrode. The salts, Na[FSA] (Mitsubishi Materials Electronic Chemicals purity >99%) and [C_3C_1pyrr][FSA] (Kanto Chemical, purity >99.9%), were dried under vacuum for 24 h at 353 K. The Na[FSA]-[C_3C_1pyrr][FSA] (C_3C_1pyrr = *N*-methyl-*N*-propylpyrrolidinium; FSA = bis(fluorosulfonyl)amide) (3:7 in molar ratio) ionic liquid was used as the electrolyte.[26] For comparison, an organic electrolyte, 1 M $NaPF_6$-EC/DMC (1:1 vol) was used in the charge-discharge tests at 298 K. Glass microfiber filter (Whatman GF/A) was impregnated with the electrolyte at 333 K under vacuum for 1 day prior to the test.

Charge-discharge tests were measured by a Hokuto Denko HJ1001SD8 charge-discharge test device. All the electrochemical measurements were conducted at least three hours after temperature adjustment in an ESPEC Environmental Test Chamber.

3. Results and Discussion

Figure 1 shows the results of Rietveld refinement for the XRD patterns of the synthesized m-$NaFePO_4$. Table 1 summarizes the corresponding crystallographic data. The refinement revealed a pure single phase of m-$NaFePO_4$, belonging to the *Pnma* space group, which agrees with previously reported data.[14] The prepared m-$NaFePO_4$ and Super C65 were thoroughly mixed by ball milling.

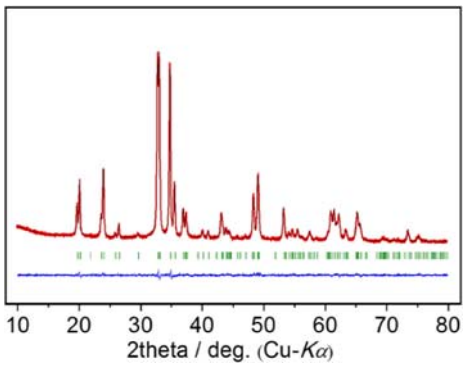

Figure 1. (Color online) Rietveld refinement result for m-$NaFePO_4$ prepared by a solid-state method. The red line indicates the observed pattern, and the black line refers to the calculated pattern. The blue line is the difference between the red and black lines. The positions of the diffraction peaks are indicated by green marks.

Table 1. Crystallographic data of the prepared m-$NaFePO_4$ by Rietveld refinement.

Chemical formula $NaFePO_4$ (S.G. *Pnma*)						
Refinement results *Chi*2 = 1.67, R_p = 0.489%, R_{wp} = 0.632%						
***a*/Å**		***b*/Å**		***c*/Å**		***V*/Å^3**
8.981445(9)		6.86687(8)		5.0441(6)		311.089(6)
Atom	Wyckoff symbol	*x*	*y*	*z*	B_{iso}/Å^2	Occup.
Fe	4*a*	0	0	0	0.5	1.0
P	4*c*	0.1751(2)	0.25	0.4556(5)	0.5	1.0
Na	4*c*	0.3453(3)	0.25	0.9689(6)	0.5	1.0
O1	8*c*	0.1180(2)	0.06698(3)	0.3267(3)	0.5	1.0
O2	4*c*	0.3491(3)	0.25	0.4576(7)	0.5	1.0
O3	4*c*	0.1222(4)	0.25	0.7457(6)	0.5	1.0

Figure 2 shows the comparison of the XRD patterns for the m-$NaFePO_4$ before and after ball milling with Super C65. The XRD measurements confirm that the ball-milled m-$NaFePO_4$ was pure, and that peak broadening was characterized by reduction of the crystallite size during milling. Figure 3 shows SEM images of the as-synthesized m-$NaFePO_4$, Super C65, and the mixture of m-$NaFePO_4$ and Super C65 after planetary ball milling, respectively. The size of the synthesized m-$NaFePO_4$ particles ranged from 500 to 250 nm. The particle size was reduced to 200 to 100 nm by ball milling. Super C65 with a particle size smaller than 50 nm was well distributed among the m-$NaFePO_4$ particles.

Figure 4 shows the results of galvanostatic charge-discharge tests for the Na/m-$NaFePO_4$ cell at 298 and 363 K with the Na[FSA]-[C_3C_1pyrr][FSA] IL electrolyte, and at 298 K with the 1 M $NaPF_6$/EC-DMC (1:1) organic electrolyte. Under the cut-off voltage of 1.5–4.5 V, the m-$NaFePO_4$ electrode exhibited a reversible capacity of

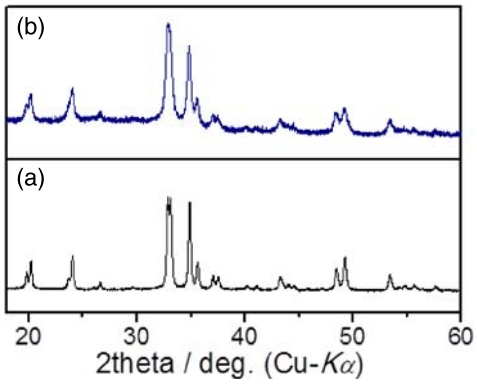

Figure 2. (Color online) X-ray diffraction patterns of m-$NaFePO_4$ (a) as synthesized and (b) after ball-milling with Super C65 for 12 hr.

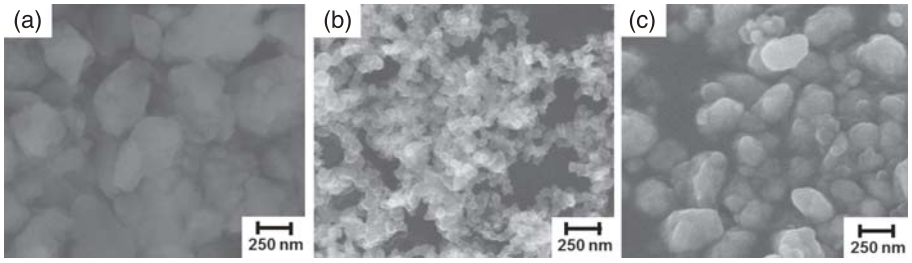

Figure 3. Field-emission SEM images (a) as prepared m-$NaFePO_4$, (b) Super C65, and (c) mixture of m-$NaFePO_4$ and Super C65 after ball-milling for 12 hr.

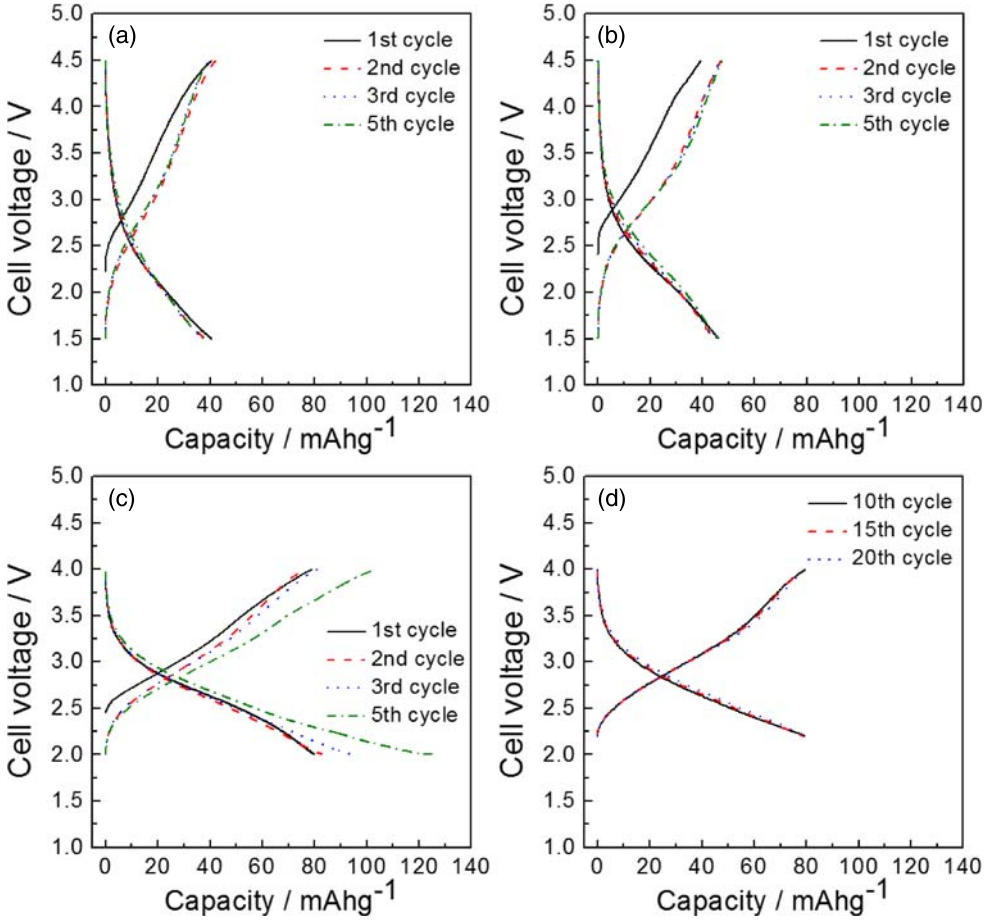

Figure 4. (Color online) Charge-discharge curves of a Na/m-$NaFePO_4$ cell (a) at 298 K in Na[FSA]-[C_3C_1pyrr][FSA] at C/20 (cut-off: 4.5–1.5 V), (b) at 298 K in 1 M $NaPF_6$/EC-DMC (1:1) at C/20 (cut-off: 4.5–1.5 V), (c) at 363 K in Na[FSA]-[C_3C_1pyrr][FSA] at C/20 (cut-off: 4.5–1.5 V), and (d) in subsequent measurement of (c) after the 9th cycle at a higher current density of C/5 (cut-off: 4.0–2.2 V).

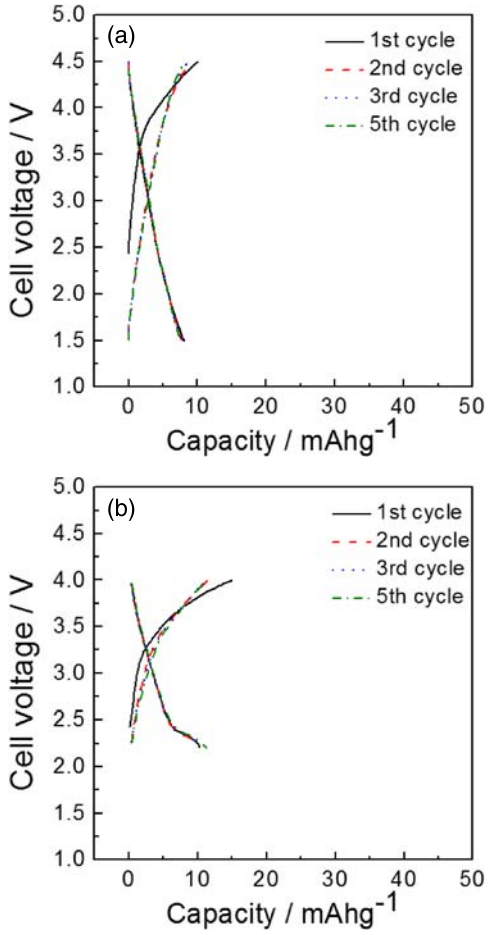

Figure 5. (Color online) Charge-discharge curves of a Na/Super C65: PTFE (50:50 wt%) cell (a) at 298 K in Na[FSA]-[C_3C_1pyrr]-[FSA] at 10 mA g^{-1} with cut-off voltage of 4.5–1.5 V, (b) at 363 K in Na[FSA]-[C_3C_1pyrr][FSA] at 10 mA g^{-1} with cut-off voltage of 4.0–2.2 V.

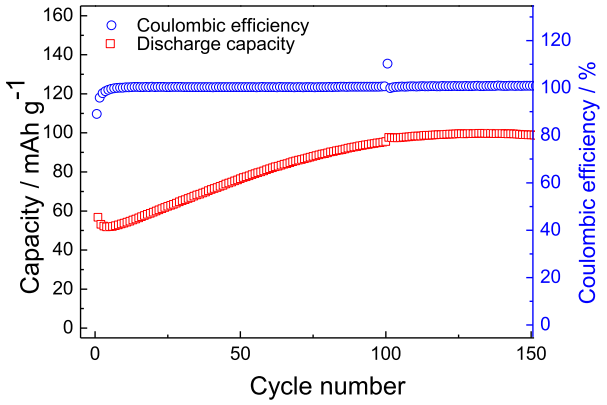

Figure 6. (Color online) Cycling performance of m-$NaFePO_4$ at 363 K in Na[FSA]-[C_3C_1pyrr][FSA] at C/2 with cut-off voltage of 4.0–2.2 V. Red and blue markers indicate discharge capacity and coulombic efficiency, respectively, at each cycle. The measurement was interrupted at the 100th cycle only, and then restarted to determine the effect of intermission.

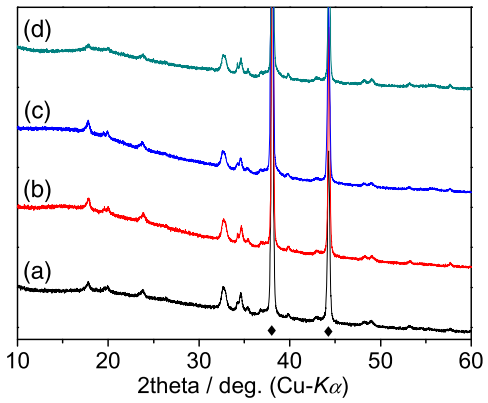

Figure 7. (Color online) Ex situ XRD patterns of the m-$NaFePO_4$ electrode (a) before charge-discharge test, (b) after the 1st cycle, (c) after the 10th cycle, and (d) after the 100th cycle. The ◆ marks indicate the peaks of Al mesh.

38 mAh g^{-1} and 40 mAh g^{-1} at a rate of C/20 (1 C = 155 mA g^{-1}) at 298 K using Na[FSA]-[C_3C_1pyrr][FSA] and 1 M $NaPF_6$/EC-DMC, respectively (Figs. 4(a) and (b)) in the 2nd cycle. Although the practical capacity was quite limited at 298 K, stable reversibility was observed during successive cycles. The charge-discharge test at 363 K in Na[FSA]-[C_3C_1pyrr][FSA] delivered a reversible capacity of 80 mAh g^{-1} in the initial discharge at a rate of C/20 (Fig. 4(c)) under a cut-off voltage of 2.0–4.0 V. The discharge capacity was doubled by merely elevating the operating temperature from 298 to 363 K. However, an irreversible capacity emerged from the 3rd discharge, despite the narrower voltage region as compared to that in the tests conducted at 298 K. This irreversible capacity probably results from the decomposition of the IL electrolyte, which is accelerated at elevated temperatures, particularly on nanosized materials, including carbon black.[37] The irreversible capacity fades upon further limiting the lower cut-off voltage from 2.0 to 2.2 V, at a current density of C/5. After this adjustment, the material exhibited stable cycle performance with a reversible capacity of 80 mAh g^{-1} by the 20th cycle (Fig. 4(d)).

Galvanostatic charge-discharge tests on Super C65 were conducted to clarify the effects of Super C65 on the capacity at intermediated temperature. Super C65 powder was also planetary ball-milled for 6 hr in Ar atmosphere which was the same conditions used for the mixture of m-$NaFePO_4$ and Super C65 ball-milled. Figure 5 shows the charge-discharge curves of the Super C65 electrode at 298 and 363 K in the Na[FSA]-[C_3C_1pyrr][FSA] IL electrolyte. The working electrode composed of 50 wt% of Super C65 and 50 wt% of PTFE, delivered 14.4 mAh g^{-1} at 298 K (cut-off: 4.5–1.5 V) and 4.5 mAh g^{-1} at 363 K (cut-off: 4.0–2.2 V). Little irreversible capacity was observed in this case because of the higher cut-off voltage of 2.2 V. In the charge-discharge test for the m-$NaFePO_4$ electrode, each electrode contained 26 wt% of Super C65, and therefore the results proved that the influence of capacity by Super C65 was at most 3 mAh g^{-1}.

Figure 6 shows the cycling performance of the Na/Na[FSA]-[C_3C_1pyrr][FSA]/m-$NaFePO_4$ cell at C/2 rate with a cut-off voltage of 4.0 and 2.2 V. The discharge capacity was 58 mAh g^{-1} at the initial discharge, which continuously increased during subsequent cycles, reaching 100 mAh g^{-1} at the 120th cycle with nearly 100% coulombic efficiency. Figure 7 shows the ex-situ XRD patterns of the m-$NaFePO_4$ electrode after the 1st, 10th, and 100th cycles. The XRD pattern before cycling is also shown for comparison. The maricite structure was maintained even after 100 cycles of charge and discharge as represented by diffraction peaks with indices 101 at 20.25°, 111 at 23.96°, 220 at 32.65°, and 301 at 34.67°. No significant peak broadening was observed, suggesting that amorphization or reduction of the crystallite diameter did not occur during the cycles. This is in contrast to the previous report which claimed phase transformation of m-$NaFePO_4$ to amorphous $NaFePO_4$ during charging.[17] Although the different fabrication methods and measurement conditions may affect the structural change along with

electrochemical reactions, the present result may indicate the reversible redox activity of m-$NaFePO_4$ without loss of its crystallinity. The reason for the increase of capacity for m-$NaFePO_4$ is not clear in the current stage. A decrease in particle size followed by Na^+ extraction and insertion processes may provide effective Na^+ pathways, since the crystallite size confirmed by XRD does not always agree with the particle size.

4. Conclusion

In summary, we demonstrated the potential activity of m-$NaFePO_4$ as a positive electrode material for Na secondary batteries using an IL electrolyte at intermediate temperature. Nonflammable Na[FSA]-[C_3C_1pyrr][FSA] electrolyte is a key component that result in good performance of m-$NaFePO_4$ at intermediate temperature. This material delivers a reversible capacity of 100 mAh g^{-1} with C/2 after 100 charge and discharge cycles at 363 K. Although the practical capacity in the present study still does not reach the theoretical value, 155 mAh g^{-1}, improvements in fabrication techniques, including control of particle size and carbon coating can further enhance the possibility of superior performance. The simple synthetic procedure, abundant constituent elements, and highest theoretical capacity among Fe-based phosphates make m-$NaFePO_4$ an attractive positive electrode material for future Na secondary batteries. Further structural study on the redox activity of crystalline m-$NaFePO_4$ is now under way. This study also suggests that many other inactive materials can be converted into active materials by a combination of nano-sizing and intermediate-temperature operation.

Acknowledgments

This study was partly supported by Advanced Low Carbon Technology Research and Development Program (ALCA) of Japan Science and Technology Agency (JST) and Japanese Ministry of Education, Culture, Sports, Science and Technology (MEXT) program “Elements Strategy Initiative to Form Core Research Center”.

References

1. M. Armand and J.-M. Tarascon, *Nature*, **451**, 652 (2008).
2. J.-M. Tarascon and M. Armand, *Nature*, **414**, 359 (2001).
3. M. R. Palacin, *Chem. Soc. Rev.*, **38**, 2565 (2009).
4. J.-M. Tarascon, *Nat. Chem.*, **2**, 510 (2010).
5. P. W. Gruber, P. A. Medina, G. A. Keoleian, S. E. Kesler, M. P. Everson, and T. J. Wallington, *J. Ind. Ecol.*, **15**, 760 (2011).
6. R. D. Shannon, *Acta Crystallogr., Sect. A*, **32**, 751 (1976).
7. Y. Fang, L. Xiao, J. Qian, X. Ai, H. Yang, and Y. Cao, *Nano Lett.*, **14**, 3539 (2014).
8. A. Yamada, *MRS Bull.*, **39**, 423 (2014).
9. Y. Zhu, Y. Xu, Y. Liu, C. Luo, and C. Wang, *Nanoscale*, **5**, 780 (2013).
10. C. Y. Chen, K. Matsumoto, T. Nohira, R. Hagiwara, Y. Orikasa, and Y. Uchimoto, *J. Power Sources*, **246**, 783 (2014).
11. P. Barpanda, T. Ye, S. Nishimura, S.-C. Chung, Y. Yamada, M. Okubo, H. Zhou, and A. Yamada, *Electrochem. Commun.*, **24**, 116 (2012).
12. H. Kim, R. A. Shakoor, C. Park, S. Y. Kim, J.-S. Kim, Y. N. Jo, W. Cho, K. Miyasaka, R. Kahraman, Y. Jung, and J. W. Choi, *Adv. Funct. Mater.*, **23**, 1147 (2013).
13. P. Barpanda, G. Liu, C. D. Ling, M. Tamaru, M. Avdeev, S.-C. Chung, Y. Yamada, and A. Yamada, *Chem. Mater.*, **25**, 3480 (2013).
14. M. Avdeev, Z. Mohamed, C. D. Ling, J. Lu, M. Tamaru, A. Yamada, and P. Barpanda, *Inorg. Chem.*, **52**, 8685 (2013).
15. S. Oh, S.-T. Myung, J. Hassoun, B. Scrosati, and Y.-K. Sun, *Electrochem. Commun.*, **22**, 149 (2012).
16. J. Kim, D. Seo, H. Kim, I. Park, J. Yoo, S. Jung, Y. Park, W. A. Goddard, III, and K. Kang, *Energy Environ. Sci.*, **8**, 540 (2015).
17. A. Sun and A. Manivannan, *ECS Trans.*, **35**, 3 (2011).
18. K. Kuratani, N. Uemura, H. Senoh, H. T. Takeshita, and T. Kiyobayashi, *J. Power Sources*, **223**, 175 (2013).
19. A. Ponrouch, R. Dedryvère, D. Monti, A. E. Demet, J. M. Ateba Mba, L. Croguennec, C. Masquelier, P. Johansson, and M. R. Palacín, *Energy Environ. Sci.*, **6**, 2361 (2013).
20. G. G. Eshetu, S. Grugeon, S. Laruelle, S. Boyanov, A. Lecocq, J.-P. Bertrand, and G. Marlairl, *Phys. Chem. Chem. Phys.*, **15**, 9145 (2013).
21. S. Wilken, P. Johansson, and P. Jacobsson, *Solid State Ionics*, **225**, 608 (2012).
22. S. Wilken, M. Treskow, J. Scheers, P. Johansson, and P. Jacobsson, *RSC Adv.*, **3**, 16359 (2013).
23. M. Armand, F. Endres, D. R. MacFarlane, H. Ohno, and B. Scrosati, *Nat. Mater.*, **8**, 621 (2009).
24. J. P. Hallett and T. Welton, *Chem. Rev.*, **111**, 3508 (2011).
25. D. R. MacFarlane, N. Tachikawa, M. Forsyth, J. M. Pringle, P. C. Howlett, G. D. Elliott, J. H. Davis, M. Watanabe, P. Simon, and C. A. Angell, *Energy Environ. Sci.*, **7**, 232 (2014).
26. K. Matsumoto, Y. Okamoto, T. Nohira, and R. Hagiwara, *J. Phys. Chem. C*, **119**, 7648 (2015).
27. C. Chen, K. Matsumoto, T. Nohira, C. Ding, T. Yamamoto, and R. Hagiwara, *Electrochim. Acta*, **133**, 583 (2014).
28. A. Fukunaga, T. Nohira, Y. Kozawa, R. Hagiwara, S. Sakai, K. Nitta, and S. Inazawa, *J. Power Sources*, **209**, 52 (2012).
29. C. Ding, T. Nohira, K. Kuroda, R. Hagiwara, A. Fukunaga, S. Sakai, K. Nitta, and S. Inazawa, *J. Power Sources*, **238**, 296 (2013).
30. C. Ding, T. Nohira, R. Hagiwara, K. Matsumoto, Y. Okamoto, A. Fukunaga, S. Sakai, K. Nitta, and S. Inazawa, *J. Power Sources*, **269**, 124 (2014).
31. C.-Y. Chen, K. Matsumoto, T. Nohira, and R. Hagiwara, *J. Electrochem. Soc.*, **162**, A176 (2014).
32. C.-Y. Chen, K. Matsumoto, T. Nohira, C. Ding, T. Yamamoto, and R. Hagiwara, *Electrochim. Acta*, **133**, 583 (2014).
33. T. Yamamoto, T. Nohira, R. Hagiwara, A. Fukunaga, S. Sakai, and K. Nitta, *Electrochim. Acta*, **211**, 234 (2016).
34. C.-Y. Chen, T. Kiko, T. Hosokawa, K. Matsumoto, T. Nohira, and R. Hagiwara, *J. Power Sources*, **332**, 51 (2016).
35. K. Matsumoto, T. Hosokawa, T. Nohira, R. Hagiwara, A. Fukunaga, K. Numata, E. Itani, S. Sakai, K. Nitta, and S. Inazawa, *J. Power Sources*, **265**, 36 (2014).
36. J. R.-Carvajal, Commission on powder diffraction (IUCr) *Newsletter*, **26**, 12 (2001).
37. C.-Y. Chen, K. Matsumoto, T. Nohira, and R. Hagiwara, *J. Electrochem. Soc.*, **162**, A2093 (2015).